NUMERICAL INVESTIGATION OF SUPERSONIC MIXING LAYERS

Qibing Li, Song Fu
Department of Engineering Mechanics,
Tsinghua University
Beijing 100084, China
lqb@tsinghua.edu.cn, fs-dem@mail.tsinghua.edu.cn

ABSTRACT

The high-speed mixing layers with convective Mach number $M_c = 0.4, 0.8$ and 1.2 are investigated numerically. The present results provide the flow-field structure, the similarity of the mean quantity distributions, the characteristic of velocity fluctuation and the normalized growth rates which all agree with experimental and other numerical results. The scaling analyse shows that the ESS prevails in the inner region of the fully developed mixing layer and compressibility affects little on the scaling exponents. This is consistent with the similar spectra of the velocity in the mixing layers with different M_c.

INTRODUCTION

Compressible turbulent mixing layers commonly occur in various engineering applications such as combustion, propulsion and environmental flows. The original work of Brown and Roshko (1974) on the structure of planar mixing layers triggered extensive computational (Vreman et al. 1996, Iwase et al. 2001, Pantano and Sarkar 2002, Kourta and Sauvage 2002) and experimental (Goebel and Dutton 1991, Gruber et al. 1993, Debisschop et al. 1994, Barre et al. 1997, Rossmann et al. 2002) research during the past three decades that substantiated the idea that large-scale structures control the dynamics of all free shear flows (Gutmark et al. 1995). With increasing convective Mach number M_c, the ratio of the free-stream velocity difference to the sum of the sound speeds, the mixing layer become highly three dimensional and the normalized growth rate decreased rapidly, reaching an asymptotic value of about 0.2 for supersonic convective Mach numbers. In high M_c mixing layer there exist unsteady shocklets which require much needed further studied.

Due to the limitation of computer capability, many of the exiting numerical simulations of the supersonic mixing layer are in 2-D or of temporal development in which the periodic conditions are applied in the streamwise direction. As turbulence is three dimensional the 2-D simulations can only provide limited information. While the temporal simulations are computationally efficient, the drawbacks are that they cannot properly account for the effects of the velocity ratio across the layer, the divergence of streamlines, the asymmetric entrainment, nor the distinct and spatially nonuniform convection of various turbulence structures.

In the present work the 3-D spatial evolving compressible mixing layers are investigated numerically with the simplified gas-kinetic BGK scheme to understand the compressibility effect in the high-speed flow. The scheme is based on the BGK-Boltzmann equation and many applications of it show the good robustness and rightness (Xu 2001). The details of the scheme and its simplification can be found in Li (2002).

Table 1: Computational parameters

Case	M_1	M_2	M_c	Re_c	Re
1	1.9	1.1	0.4	375	200
2	2.9	1.3	0.8	525	400
3	3.5	1.1	1.2	575	600

COMPUTATIONAL PARAMETERS

In the present simulation the same grid system of uniformly spaced in the x and z direction and stretched in the y direction is employed for the three cases. The computational domain size is defined as $(L_x \times L_y \times L_z) = 350 \times 120 \times 30$ with $(N_x \times N_y \times N_z) = 875 \times 200 \times 80$ grid points. The ratio of the maximal cell size to the minimal size ($\Delta y_{min} = 0.2$) is 10.5.

All variables are nondimensionallized by the initial vorticity thickness $\delta_\omega(0)$, the high-speed side free stream parameters $\rho_1, a_1, \rho_1 a_1^2$. The initial momentum thickness is given as $\delta_m(0) = 0.25$. The free stream sound speed is set to $a_1 = a_2 = 1$, and pressure $p_1 = p_2 = 1/\gamma$, where gas constant $\gamma = 1.4$. The kinematic viscosity $\nu = 0.001$ is used for all of the simulations. Table 1 provides the computational parameters of three cases where Re_c and Re are Reynolds numbers based on $U_c = 0.5(U_1 + U_2)$ and $\Delta U = U_1 - U_2$ respectively. The present computational domains are large enough for the flow to achieve fully developed state, as when $x = L_x$, $x_{\rm eff}/\delta_{m1}$ are all larger than 1500, where $x_{\rm eff} = x(1 - U_2/U_1)$, δ_{m1} is the momentum thickness of the high-speed stream set to half of the total thickness here. The criterion for $x_{eff}/\delta_{m1} > 500$ was proposed by Papamoschou and Roshko (1988).

At the inflow boundary ($i = 1$), the flow quantities, such as density, velocity, and pressure are prescribed, but a broadband forcing (Stanley and Sarkar 1997) is also superimposed at the inlet to generate early development of the shear layer. For the outflow ($i = i_{\max}$) and the two lateral side boundaries ($j = 1$ and $j = j_{\max}$), Thompson's non-reflecting boundary conditions are employed. For the outflow boundary, the pressure correction discussed by Poinsot and Lele (1992) is also applied.

The streamwise velocity profile of the inflow is given by the hyperbolic tangent function,

$$u(y) = 0.5(U_1 + U_2) - 0.5(U_1 - U_2)\tanh[0.5y/\delta_m(0)]. \quad (1)$$

The simulation is started with an initialized flow field in which the streamwise velocity is determined by Eq. (1) and the transverse velocity is fixed as zero value. The density and pressure fields are uniform throughout the flow field.

RESULTS

Statistics and Compressibility

The statistics is processed in the time about six times of the maximal time scale $T = L_x/U_c$. Figure 1 shows the development of the mixing layers where one can see that the mixing layer reaches linear region after some distance from the upstream and the center of the mixing layer leans to the low speed side which is often found in experiments and can not be catched in the simulations of temporal development mixing layer. With increasing convective Mach number, the mixing layer shows more stable, thus much longer streamwise distance needed to become turbulence. But the shift of the center increases indeed.

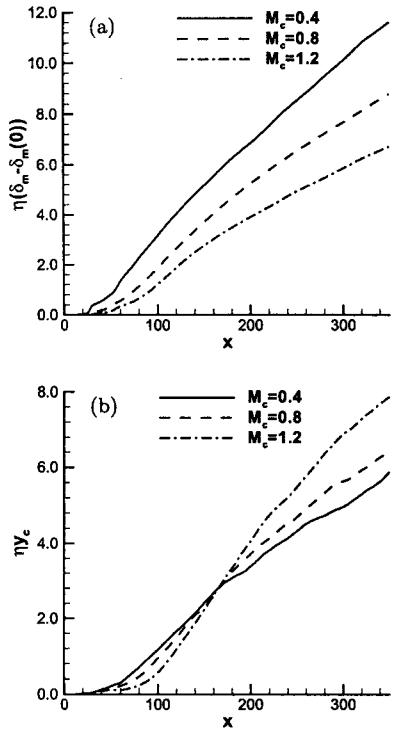

Figure 1: Development of mixing layers with different M_c: (a) the normalized momentum thickness and (b) the center of mixing layer. y_c is the center of mixing layer where $\overline{u}$ is equal to U_c. The normalizing factor is defined as $\eta = (U_1 + U_2)/(U_1 - U_2)$.

The normalized growth rates (shown in Fig.2) calculated from the momentum thickness in the fully developed region decrease evidently with increasing M_c which agree well with existing numerical (Day et al. 1998, Pantano and Sarkar 2002) and experimental (Papamoschou and Roshko 1988, Goebel and Dutton 1991, Debisschop et al. 1994, Barre et al. 1997, Rossmann et al. 2002) studies.

It is well known that developed turbulent mixing layer evolves self-similarly which can be verified in Fig. 3. The collapse of the data is excellent and the present results show a good agreement with either numerical results of Pantano and Sarkar (2002) (M_c = 0.3), Rogers and Moser (1994) or experiment data of Bell and Mehta (1990). The latter two are on the incompressible shear layers. A test case is calculated with the same parameters as case 1 except for the coarser computational mesh to examine the level of grid dependency. The cell size is about one and a half times larger than that in case 1. Figure 3 shows the comparisons of the coarse and fine grid results at different streamwise

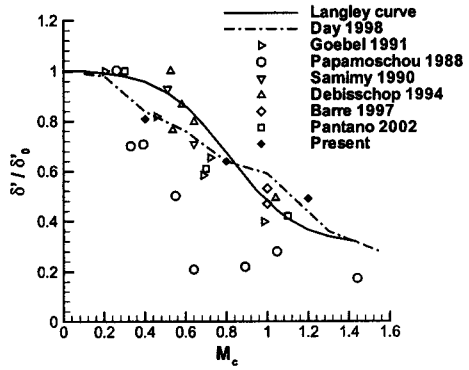

Figure 2: Growth rates of mixing layers with different M_c where δ'_0 is the incompressible mixing layer growth rate.

locations. The results on different computational mesh vary little showing the present grid adequate in resolving the main flow features.

The maximal velocity fluctuation intensity decreases with increasing convective Mach number, especially for the transverse one and the shear stress (see Fig. 4). Compressibility restrains the transverse fluctuation strongly which leads to the decrease of the shear stress, thus the growth rate of the mixing layer decreases. The present calculations are in good agreement with existing results such as (Elloit and Samimy 1990, Goebel and Dutton 1991, Debisschop et al. 1994, Barre et al. 1997, Urban and Mungal 2001, Stanley and Sarkar 1997, Pantano and Sarkar 2002) except that the shear stress shows a little larger which may come from that the present mesh size is not small enough to resolve the smallest fluctuation, leading to small dissipation.

Figure 5 shows that the ratio between the shear stress and the turbulent energy keeps constant ($\approx$ 0.35) in the inner regime of the mixing layer, which agree well with the experimental result in Elloit and Samimy (1990) and Debisschop et al. (1994). According their view, this value is very important to the study of turbulent closure. A constant ratio between the turbulent shear and the kinetic energy means all the length scales are equally affected by the compressibility or supersonic character of the flows. The increase with M_c in the outer regime maybe come from the complex Mach waves outside the mixing layer.

In the mixing layer the velocity fluctuation shows strong intermittence, especially in the layer boundary region. There are more fluctuations with large negative amplitude in the high speed side region of the mixing layer and on the contrary more large positive amplitude fluctuations on the other side. The present result agrees well with these experimental observations. With increasing M_c the intermittence increases and the position with the peak value moves outwards which reveals the decreasing growth rate and the dramatic variation of the flow near the layer boundary.

Coherent structure in mixing layer

Figure 7 shows the isosurface of Q, the second invariant of $\nabla\vec{u}$, in the mixing layer upstream. It is seen there that 3-D large structures develops from the statistically 2-D flows. The flow loses its stability quickly in the upstream region, then vortices occur, roll up and interact with each other while moving downstream. The flow instability is dominated by the spanwise rollers when $M_c = 0.4$, similar to the incompressible results of Iwase et al. (2001), while oblique

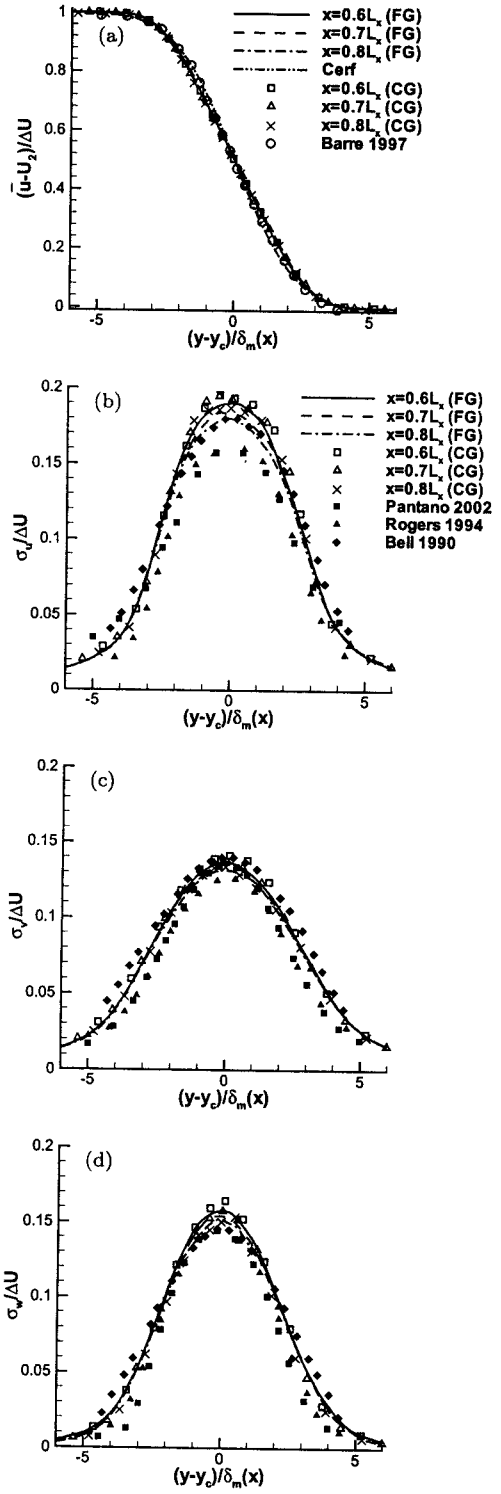

Figure 3: Profiles of the mean streamwise velocity (a) and the velocity fluctuation intensity (b,c,d) at different locations ($M_c = 0.4$). 'Cerf' is the error function profile which is the first order approximation to the mean streamwise velocity in incompressible mixing layer. The symbol 'FG' represents the results calculated on the fine grid and 'CG' on the coarse grid.

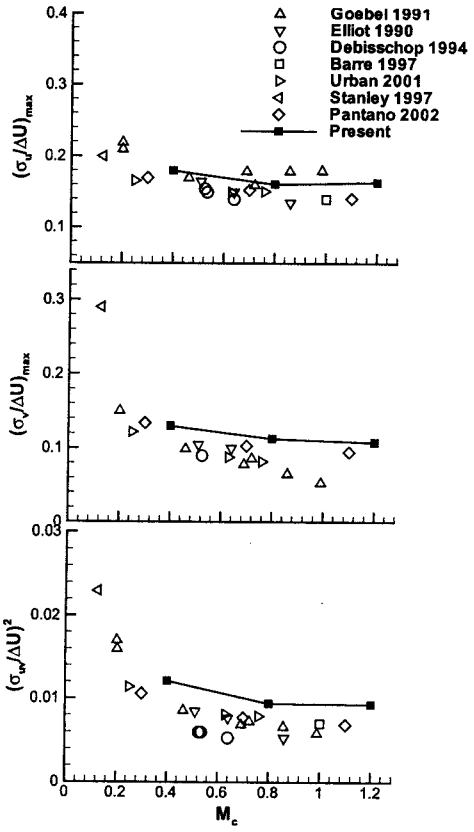

Figure 4: Maximal velocity fluctuation intensity of the mixing layers with different M_c.

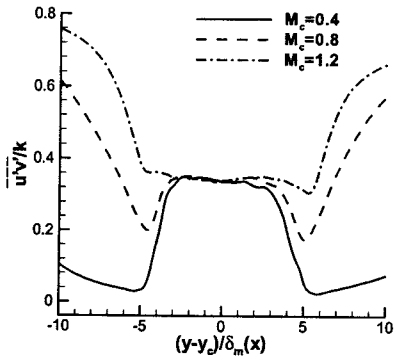

Figure 5: The ratio of shear stress to turbulent energy in mixing layers with different M_c.

structures play a much prominent role when $M_c = 1.2$. From the isosurface of Q, one can also observe the rib structures between rollers in low M_c mixing layer. But complex Mach waves were not easily identifiable from the isosurface of Q at high M_c case although they are evidently seen easily in the plots of pressure contours (see Fig. 8). In the mixing layer with high convective Mach number, there may exist shocklets (Rossmann et al. 2002). It is difficult to find a weak shock in a 3-D flow and this requires further studied.

The information of vortex evolution can be further found from the energy spectrum. Figure 9(a) shows the power spectrum of streamwise velocity at different positions along

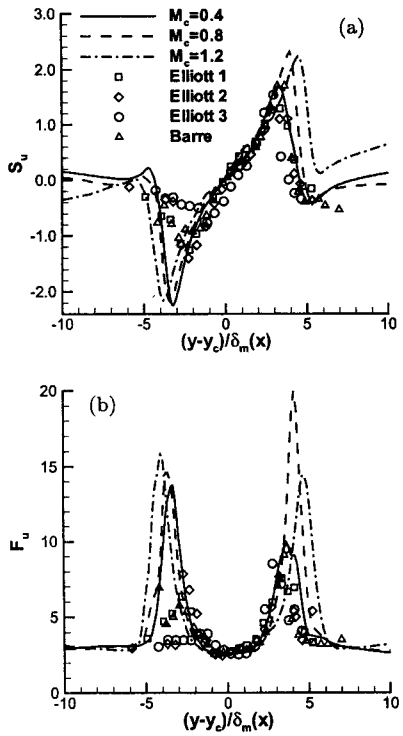

Figure 6: Skewness and flatness factors distribution of the streamwise velocity. The convective Mach numbers for 'Elliott 1, 2, 3' and 'Barre' are 0.51, 0.64, 0.86 and 1.0 respectively.

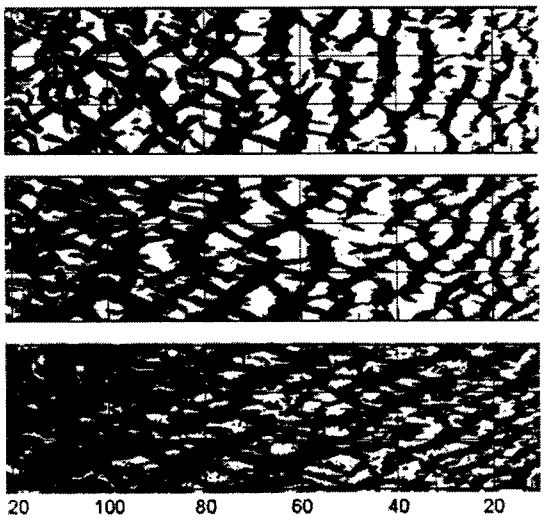

Figure 7: Isosurface of the second invariant of $\nabla\vec{u}$ (Top view, $Q = 0.01$). From top to bottom, the pictures are for $M_c = 0.4, 0.8$ and 1.2 respectively.

the geometric centerline ($y = 0$). At $x = 0.1L_x$ the vortex have begun rolling up, the spectrum is dominated by some discrete modes corresponding to the first subharmonic ($St = 0.02$). Here the Strouhal number is defined as $St = f\delta_m(0)/U_c$. At the downstream station, the spectrum shows a shift in the peak to low wavenumbers and becomes broad which show the growth in the streamwise. A spectral slope about $-5/3$ can be seen which suggests the flow has

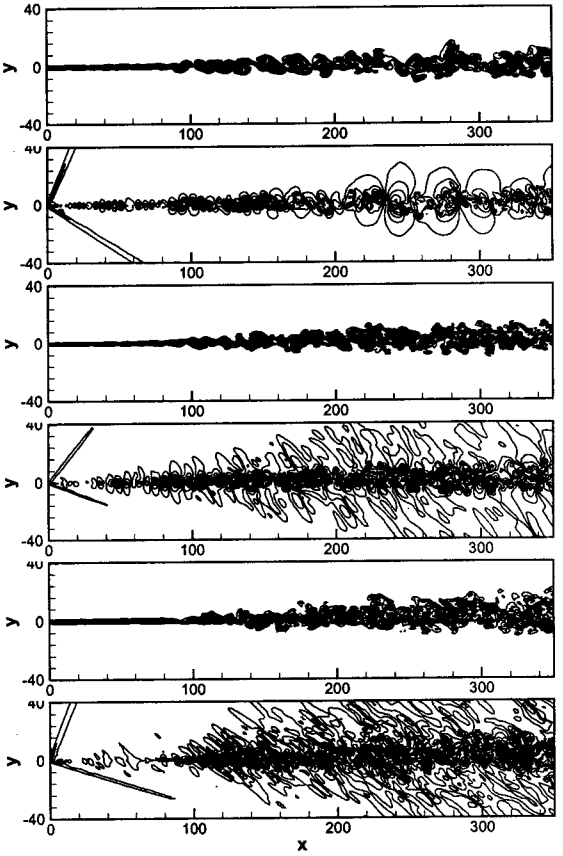

Figure 8: Instantaneous vorticity and pressure contours on a spanwise section in the mixing layer with different M_c. From top to bottom, the first tow pictures are the vorticity and pressure distribution for $M_c = 0.4$ and the next four are for $M_c = 0.8$ and $M_c = 1.2$ respectively.

achieved full development. The spectrum peaks near the subharmonics are the result of low-frequency jitter in the locations of vortex roll up and pairing which commonly occur in the naturally developing mixing layer. The spectra in different transverse regions of a mixing layer are also different in the low-frequency part (see Figure 9b). From the high-speed side to the low-speed side, the peak of the spectrum is shift to the low-frequency direction and the slope becomes larger gradually. These show that the large-scale structures absorb energy mainly from the free streams, thus they are dominated by the free streams. These also show that the structures move with different velocities in different regions and may be teared up by the strong shearing in a high M_c mixing layer.

From figure 9(c) one can find that the spectrum of the transverse and spanwise fluctuant velocity are similar to each other and both look like the streamwise velocity spectrum, especially for the high-frequency part. But their slopes of the low-frequency are slower, showing the anisotropy of the large-scale fluctuation. This comes from the fact that the turbulence energy is transported from the streamwise direction to the transverse direction and redistributed to the spanwise direction. The spectrum of pressure shows some more distinct peaks which means the large structures can be effectively described by pressure. In the mixing layers with different M_c, the streamwise velocity spectra are similar except for the peak positions in the low-frequency part

(see Figure 9d). That is, compressibility mainly affects large-scale fluctuations.

The present results show that in the inner region of the fully developed mixing layer, the ESS (extended self-similarity) (see Benzi 1995, She and Leveque 1994) prevails. The pth-order velocity structure functions are defined as

$$S_p(l) =< |\delta v_l|^p >= \int_{-\infty}^{\infty} |\delta v_l|^p P(\delta v_l) d(\delta v_l), \qquad (2)$$

where $\delta v_l = v(t+l) - v(t)$ is a velocity increment across a distance l. Here the Taylor's frozen turbulence hypothesis is used, as the root-mean-square velocity fluctuations are typically only 15% of the mean velocity difference of the free streams. Figure 10(a) shows the extended self-similarity in the inner region downstream of the mixing layer with $M_c = 0.4$. The power law can be found from the linear dependence of $S_p(l)$ on $S_3(l)$ which shows the ESS in this region. It is notable that the range of l for which the power law behavior of $S_p(l) \propto l^{\zeta_p}$ can hardly be observed due to the low Reynolds number.

The scaling exponents ζ_p are shown in figure 11 which come from the least square fits of the ESS curves. To consider the convergence of ζ_p with the sample size of the data, the exponents are calculated with three-seventh, five-seventh and the full sample size in the mixing layer with $M_c = 0.4$: the ζ_p values decrease as the sample size increases. A smaller value of ζ_p means a larger departure from a Kolmogorov 1941 value, and hence larger intermittency effects. This is because as the sample size increase, larger fluctuation amplitudes are included. The present results show that even for $p = 15$, ζ_p has converged within 1.6% for 3/7 sample size and 0.2% for 5/7 sample size (symbols in figure 11 overlap). Thus the present data size is adequate. With increasing convective Mach number M_c, the ζ_p presents only a little decrease revealing the increasing intermittency effects, which is consistent with previous discussion. The present results show that compressibility affects little on the scaling exponents. The values is between the K41 value and the SL model which is understandable since the latter two are derived under the condition of homogeneous and isotropy.

CONCLUSION

The supersonic mixing layer with convective Mach number $M_c = 0.4, 0.8$ and 1.2 are studied numerically. The numerical results here provide the flow-field structure, the characteristic of velocity fluctuation and the normalized growth rates which are all in good agreement with experimental and other numerical results. The ESS prevails in the inner region of the fully developed mixing layer and compressibility affects little on the scaling exponents, which is consistent with the similar spectra of the velocity of the mixing layers with different M_c.

REFERENCES

Barre, S., Braud, P., Chambres, O. and Bonnet, J. P., 1997, "Influence of inlet pressure conditions on supersonic turbulent mixing layers", *Exp. Therm. Fluid Sci.*, Vol. 14, pp. 68-74.

Bell, J. H. and Mehta, R. D., 1990, "Development of a two-stream mixing layer from tripped and untripped boundary layers", *AIAA J.*, Vol. 28, pp. 2034-2042.

Benzi, R., Ciliberto, S., Baudet, C. and Chavarria, G. R., 1995, "On the scaling of 3-dimensional homogeneous and isotropic turbulence", *Physica D*, Vol. 80, pp. 385-398.

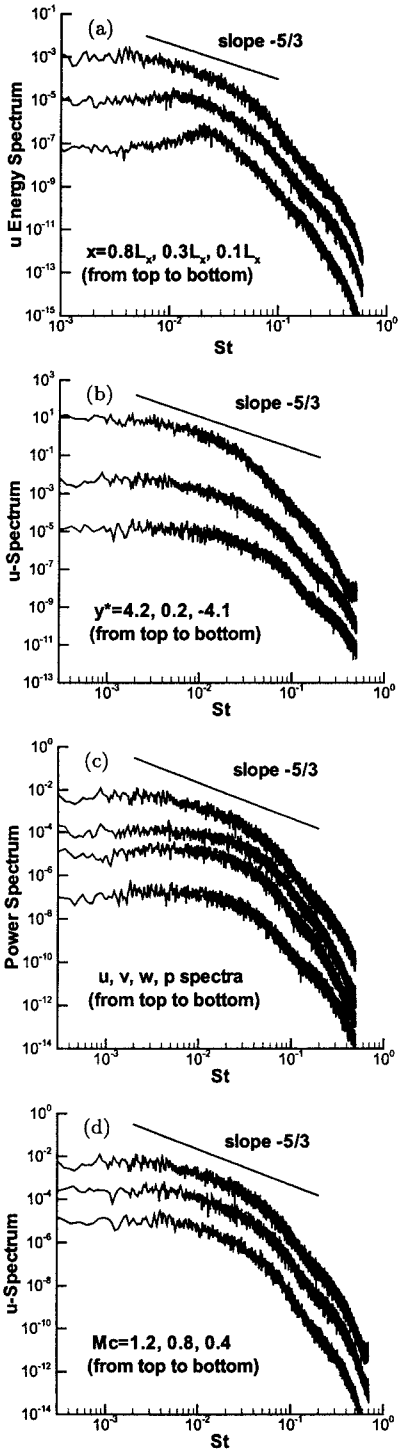

Figure 9: Power spectra: streamwise velocity spectrum at different locations on the line $y = 0$ ($M_c = 0.4$) (a) and $x = 0.8L_x$ ($M_c = 1.2$) (b); (c) shows the velocity and pressure spectrum at $x = 0.8L_x, y^* = 0.2$ with $M_c = 1.2$; (d) presents the streamwise velocity spectra in the inner region of the mixing layers ($x = 0.8L_x$, $y^* = 0.2, -0.7, -0.4$, respectively) for different M_c. For clarity, the spectra are divided by the factors: 50 at $x = 0.1L_x$ and 10^3 at $x = 0.3L_x$ in (a); 10 at $y^* = -4.1$ and 10^{-4} at $y^* = 4.2$ in (b); 10 for v-spectrum, 10^2 for w-spectrum and 10^3 for p-spectrum in (c); 10 for $M_c = 0.8$ and 10^2 for $M_c = 0.4$ in (d).

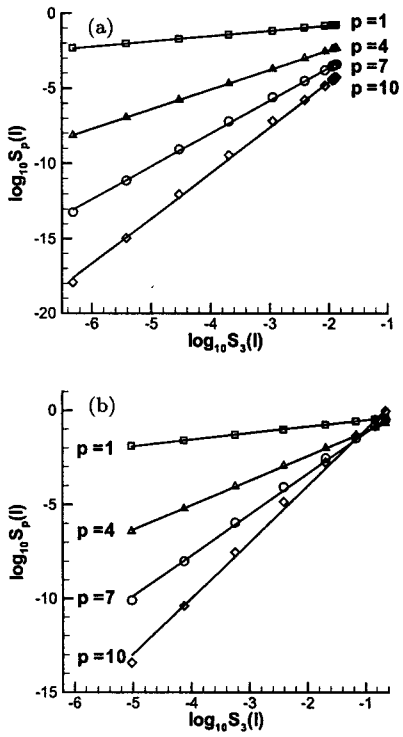

Figure 10: ESS over a range of scale of more than four decades ($2^1\delta \leq l \leq 2^{15}\delta$) where δ is the distance between the sample points in the mixing layers with (a) $M_c = 0.4$ and (b) $M_c = 1.2$. These curves are made with 3×10^5 and 6×10^5 data points recorded at the locations $y^* = -0.4$ and 0.2 ($x = 0.8L_x$) respectively. The lines are the least square fits from which the scaling exponents are extracted.

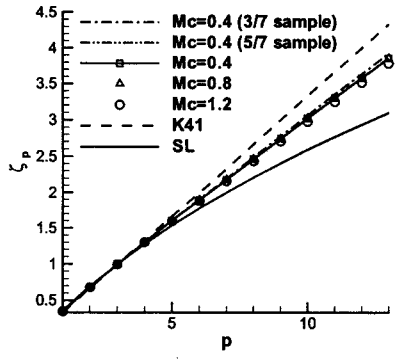

Figure 11: Structure function exponents ζ_p for the mixing layer with different M_c. The data are recorded at the locations at $y^* = -0.4$, -0.7 and 0.2 ($x = 0.8L_x$) with sample size 3×10^5, 4×10^5 and 6×10^5 respectively. The symbol 'K41' represents the Kolmogorov 1941 value and 'SL' the She-Leveque model with $\beta = (2/3)^{1/3}$ and $\gamma = 1/9$ for fully developed turbulent flow.

Brown, G. L. and Roshko, A., 1974, "On density effects and large structures in turbulent mixing layers", *J. Fluid Mech.*, Vol. 64 (4), pp. 775-816.

Day, M. J., Reynolds, W. C. and Mansour, N. N., 1998, "The structure of the compressible reacting mixing layer: insights from linear stability analysis", *Phys. Fluids*, Vol. 10, pp. 993-1007

Debisschop, J. R., Chambres, O. and Bonnet, J. P., 1994, "Velocity field characteristics in supersonic mixing layer", *Exp. Therm. Fluid Sci.*, Vol. 9, pp. 147-155.

Elloit, G. S. and Samimy, M., 1990, "Compressibility effects in free shear layers", *Phys. Fluids A*, Vol. 2 (7), pp. 1231-1240.

Freund, J. B., Lele, S. K. and Moin, P., 2000, "Compressibility effects in an turbulent annular mixing layer: Part 1. turbulence and growth rate", *J. Fluid Mech.*, Vol. 421, pp. 229–267.

Goebel, S. G. and Dutton, J. C., 1991, "Experimental study of compressible turbulent mixing layers", *AIAA J.*, Vol. 29, pp. 538-546.

Gruber, M. R., Messersmith, N. L. and Dutton, J. C., 1993, "Three -dimensional velocity field in a compressible mixing layer", *AIAA J.*, Vol. 31 (11), pp. 2061-2067.

Gutmark, M.R., Schadow, K.C. and Yu, K.H., 1995, "Mixing enhancement in supersonic free shear flows", *Annu. Rev. Fluid Mech.*, Vol. 27, pp. 375-417

Iwase, S., Tanahashi, M. and Miyauchi, T., 2001, "Large scale structure and coherent fine scale eddies in high reynolds number turbulent mixing layers", *Turbulence and shear flow phenomena (Second international symposium)*, E. Lindborg et al., ed., KTH, Stockholm, pp. 131-136.

Kourta, A. and Sauvage, R., 2002, "Computation of supersonic mixing layers", *Phys. Fluids*, Vol. 14 (11), pp. 3790-3797.

Li, Q. B., 2002, "Numerical Study of Compressible Mixing Layer with BGK Scheme", Ph.D. Thesis, Tsinghua University, Beijing.

Pantano, C. and Sarkar, S., 2002, "A study of compressibility effects in the high-speed turbulent shear layer using direct simulation", *J. Fluid Mech.*, Vol. 451, pp. 329-371.

Papamoschou, D. and Roshko, A., 1988, "The compressible turbulent shear layer: an experimental study", *J. Fluid Mech.*, Vol. 197, pp. 453-477.

Poinsot, T. J. and Lele, S. K., 1992, "Boundary conditions for direct simulations of compressible viscous flows", *J. Comput. Phys.*, Vol. 101, pp. 104-129.

Rogers, M. M. and Moser, R. D., 1994, "Direct simulation of a self-similar turbulent mixing layer", *Phys. Fluids*, Vol. 6 (2), pp. 903-923.

Rossmann, T., Mungal, M. G. and Hanson, R. K., 2002, "Evolution and growth of large-scale structures in high compressibility mixing layers", *J. Turbulence*, Vol. 3, 009.

She, Z.-S. and Leveque, E., 1994, "Universal scaling laws in fully developed turbulence", *Phys. Rev. Lett.*, Vol. 72, pp. 336-339.

Stanley, S. and Sarkar, S., 1997, "Simulations of spatially developing two-dimensional shear layers and jets", *Theoret. Comput. Fluid Dynamics*, Vol. 9, pp. 121–147.

Urban, W. D. and Mungal, M. G., 2001, "Planar velocity measurements in compressible mixing layers", *J. Fluid Mech.*, Vol. 431, pp. 189-222.

Vreman, A. W., Sandham, N. D. and Luo, K. H., 1996, "Compressible mixing layer growth rate and turbulence characteristics", *J. Fluid Mech.*, Vol. 320, pp. 235–258.

Xu, K., 2001, "A gas-kinetic BGK scheme for the Navier-Stokes equations, and its connection with artificial dissipation and Godunov method", *J. Comput. Phys.*, Vol. 171, pp. 289-335.